

Physical and Gas Transport Properties of Asymmetric Hyperbranched Polyimide-Silica Hybrid Membranes

Masako Miki¹, Yasuyuki Ishikawa², Masaya Haraguchi² and Yasuharu Yamada^{3,*}

¹R&D Center for Nanomaterials and Devices, Kyoto Institute of Technology, Matsugasaki, Sakyo-Ku, Kyoto, 606-8585, Japan

²Department of Biomolecular Engineering, Kyoto Institute of Technology, Matsugasaki, Sakyo-Ku, Kyoto, 606-8585, Japan

³Institute of Technological Research, Kanagawa University, 3-27-1 Rokkakubashi, Kanagawa-ku, Yokohama, 226-8686, Japan

Abstract: Physical and gas transport properties of the asymmetric hyperbranched polyimide (HBPI) -silica hybrid membranes prepared with a dianhydride, 4,4'-(hexafluoroisopropylidene)diphthalic anhydride (6FDA), and an asymmetric triamine, 2,4,4'-(triaminodiphenyl)ether (TADE), were investigated and compared with those of the symmetric HBPI-silica hybrid membranes prepared with a symmetric triamine, 1,3,5-tris(4-aminophenoxy)benzene (TAPOB). The HBPI-silica hybrid membranes were prepared via sol-gel reaction using hyperbranched polyamic acid of which end groups were modified with silane coupling agents, water and tetramethoxysilane. The thermal mechanical and dynamic mechanical analysis measurements confirmed that the rigidity of asymmetric HBPI was higher than that of symmetric HBPI because of the rigid and asymmetric structure of TADE monomer. In addition, the degree of branching of asymmetric HBPI is lower than that of symmetric HBPI because of the different reactivity of the three amino groups included in TADE. The rigidity and linearity of HBPIs had an effect on the progression of sol-gel reaction, consequently the gas transport properties. The increasing of the gas permeability coefficient of the asymmetric dianhydride(DA)-HBPI-silica hybrid membranes with increasing silica content was smaller than those of symmetric DA- and amine(AM)-HBPI-silica hybrid membranes. In addition, the gas permeability coefficient of the asymmetric AM-HBPI-silica hybrid membranes decreased with increasing silica content. This was due to the fact that the dispersibility of silica in the asymmetric HBPI-silica hybrids, of which polymer chain was more rigid and linear than those of symmetric HBPI-silica hybrid, was not as fine as in the symmetric HBPI-silica hybrids, and that the long and tortuous diffusion path was newly formed by hybridization with silica.

Keywords: Hyperbranched Polyimide, Silica hybrid, Gas permeability, Asymmetric, Symmetric.

1. INTRODUCTION

Aromatic polyimide (PI) is one of the super engineering plastics which have been used in many high-technology fields. Especially, in recent years, aromatic PI have been of great interest in gas separation membranes because of their excellent mechanical and thermal property, and high gas permeability and selectivity [1-4]. PIs can take various kinds of structures by combining various monomers (diamines and dianhydrides).

For the asymmetric type PIs prepared from asymmetric dianhydrides and symmetric diamines, it has been reported that the resulting PIs exhibited increased solubility, reduced viscosity, and higher glass transition temperatures (T_g s) than the symmetric type PIs. The increased T_g s were ascribable to their rigid and bent structure, and the steric hindrance [5-8]. In general, it is said that the increase in gas permeability is also induced by the rigid molecular chain.

Hyperbranched polymers are highly branched three-dimensional dendritic polymers possessing unique properties (e.g., good solubility, reduced viscosity, higher fractional free volume, and multifunctionality) arising from multiple end groups. Hyperbranched polyimides (HBPIs) can be synthesized from either the self-polycondensation of AB_2 -type monomers or the polycondensation reaction of $A_2 + B_3$ monomers, where A_2 represents a dianhydride monomer and B_3 represents a triamine monomer. In the case of an $A_2 + B_3$ type polycondensation reaction, a variety of HBPIs can be synthesized by changing the monomer ratio and combining A_2 and B_3 monomers [9-11]. Fang *et al.* were the first to report the synthesis of HBPIs derived from a triamine, tris(4-aminophenyl)amine (TAPA), and commercially available dianhydrides [12,13]. We have also studied physical and gas transport properties of the HBPI membranes which have benzene ring-centered symmetric structure; i.e. we have synthesized the HBPIs by polycondensation reaction of 4,4'-(hexafluoroisopropylidene) diphthalic anhydride (6FDA) as a dianhydride monomer and triamine monomers, 1,3,5-tris(4-aminophenoxy) benzene (TAPOB), 1,3,5-tris(4-aminophenoxy) triazine (TAPOTZ) and 1,3,5-

*Address correspondence to these authors at the Institute of Technological Research, Kanagawa University, 3-27-1 Rokkakubashi, Kanagawa-ku, Yokohama, 226-8686, Japan; Tel/Fax: +81 45 481 5661; E-mail: ss503522rt@kanagawa-u.ac.jp

tris(4-aminophenyl)benzene (TAPB) and found that the HBPI(6FDA-TAPB) membranes exhibit the highest gas permeability coefficient arising from the highest fractional free volume (FFV) [14].

Additionally, we have studied the syntheses and gas transport properties of symmetric HBPI-silica hybrid membranes. Organic-inorganic hybrid materials have been recognized as a new class of high performance materials because they combine the advantages of the inorganic material (e.g., rigidity and thermal stability) and the organic polymer (e.g., flexibility, dielectric, ductility, and processability) [15, 16]. The synthesis of PI-silica hybrid materials and the investigation of their physical and gas transport properties have also received much attention [17-19]. In our previous researches about the symmetric HBPI-silica hybrid membranes, we found that the gas permeability and CO₂/CH₄ selectivity of these membranes prepared *via* sol-gel reaction using tetramethoxysilane (TMOS) increased with increasing silica content, suggesting the characteristic distribution and interconnectivity of free volume holes created by the incorporation of silica [14, 20-26].

In this study, physical and gas transport properties of the asymmetric HBPI-silica hybrid membranes prepared with a dianhydride, 6FDA, and a asymmetric triamine, 2,4,4'-(triaminodiphenyl)ether (TADE), were investigated and compared with those of symmetric HBPI-silica hybrid membranes prepared with a symmetric triamine, TAPOB.

2. EXPERIMENTAL

2.1. Materials

TAPOB was synthesized by the reduction of 1,3,5-tris(4-nitrophenoxy)benzene with palladium carbon and hydrazine in methanol[27]. Triamine monomer, TADE, and dianhydride monomer, 6FDA, were kindly supplied from Wakayama Seika Kogyo Co. (Wakayama, Japan) and Daikin Industries (Osaka, Japan), respectively. TMOS was purchased from AZmax, Co., Ltd (Tokyo, Japan). 3-Aminopropyltrimethoxysilane (APTTrMOS) and 3-(triethoxysilyl)propyl succinic anhydride (TEOSPSA) were purchased from Sigma-Aldrich Co. LLC. (St. Louis, MO, USA) and Gelest Inc. (Morrisville, PA, USA), respectively. *N,N*-Dimethylacetamide (DMAc) used as a solvent was purchased from Nacalai Tesque (Kyoto, Japan). The chemical structures of the monomers, silane coupling agents and silicon alkoxide are shown in Figure 1.

2.2. Polymerization

2.2.1. Dianhydride-Terminated Hyperbranched Polyamic Acids (DA-HBPAA)

Three mmol of 6FDA was dissolved in 30-40 ml of DMAc in a 100-ml three-neck flask under N₂ flow at room temperature. 1.6 mmol of triamine (TADE or TAPOB) in 20 ml of DMAc was then added dropwise through a syringe with stirring. The monomer content was controlled to ca. 3.5 wt%. After stirring for 3 h, 0.4 mmol of APTTrMOS as a coupling agent was added into the reaction mixture with further stirring for 1 h to afford

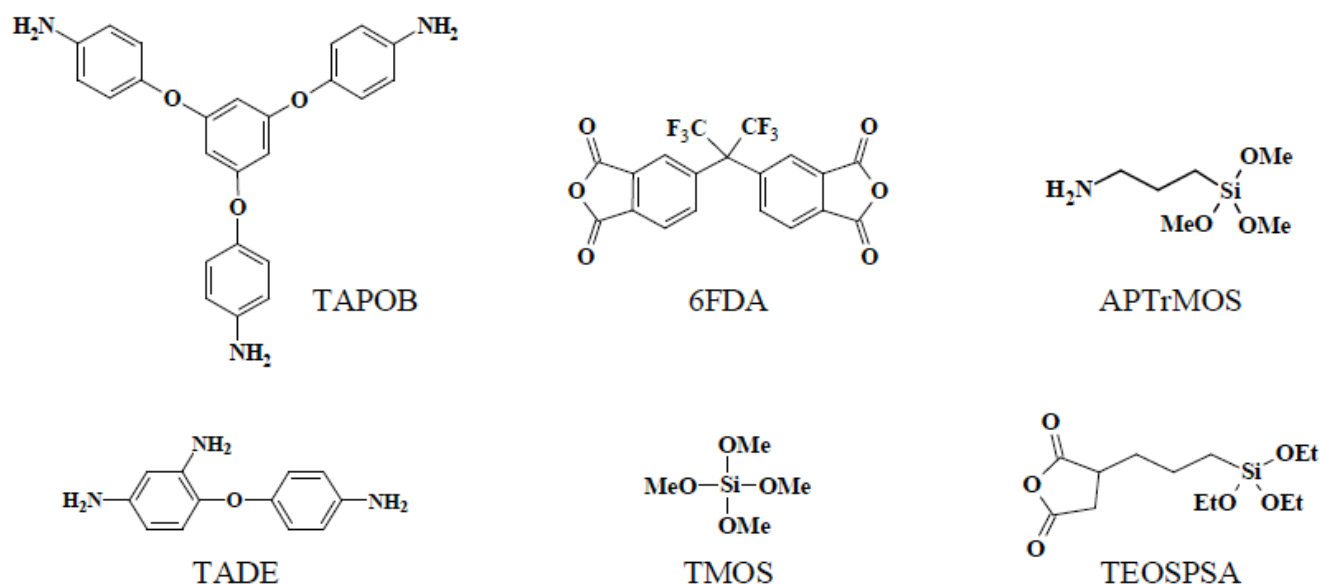


Figure 1: Chemical structures of monomers, silane coupling agents, and silicon alkoxide.

asymmetric and symmetric DA-HBPAA. The degree of terminal modification was 1/3.

2.2.2. Amine-Terminated Hyperbranched Polyamic Acids (AM-HBPAA)

Three mmol of triamine (TADE or TAPOB) was dissolved in 30-34 ml of DMAc in a 100-ml three-neck flask under N₂ flow at room temperature. 3.0 mmol of 6FDA in 28-40 ml of DMAc was then added dropwise through a syringe with stirring. The monomer content was controlled to ca. 3.5 wt%. After stirring for 3 h, 1.0 mmol of TEOSPSA as a coupling agent was added into the reaction mixture with further stirring for 1 h to afford asymmetric and symmetric AM-HBPAA. The degree of terminal modification was 1/3.

2.3. Membrane Formation

The asymmetric and symmetric HBPI-silica hybrid membranes were prepared by the reaction of asymmetric or symmetric HBPAAs with silicon alkoxide, TMOS, *via* sol-gel reaction, and then followed by thermal imidization. Appropriate amounts of TMOS and deionized water (TMOS : deionized water = 1 : 6 as a molar ratio) were added into the DMAc solution of the asymmetric or symmetric HBPAAs. The mixed solutions were stirred for 24 h and then cast on PET films and dried at 85°C for 3 h. These prepared membranes were peeled off and subsequently imidized and hybridized at 100°C for 1 h, 200°C for 1 h, and 300°C for 1 h in a heating oven under N₂ flow. The average thickness of the asymmetric or symmetric HBPI-silica hybrid membranes was about 30 μm.

2.4. Measurements

The inherent viscosity (η_{inh}) of HBPAAs was measured in a DMAc solution with a 0.5 g/dL concentration at 25°C with an Ubbelohde viscometer. Attenuated total reflection Fourier transform infrared (ATR FT-IR) spectra were recorded on a JASCO FT/IR-4100 (Tokyo, Japan) at a wavenumber range of 550–4000 cm⁻¹ and a resolution of 1 cm⁻¹. Optical transmittances (ultraviolet-visible spectroscopy) were measured with a JASCO V-530 UV/vis spectrometer at wavelengths of 200–800 nm. Thermal mechanical analysis (TMA) measurements were carried out using a Seiko Instruments TMA/SS6100 (Chiba, Japan) at a heating rate of 5°C/min under N₂ flow. Dynamic mechanical analysis (DMA) measurements were performed with a Seiko Instruments DMA6100 at a heating rate of 5°C/min under N₂ flow; the load frequency was 1 Hz. Thermogravimetric-differential

thermal analysis (TG-DTA) experiments were performed with a Seiko Instruments TG/DTA5200 at a heating rate of 10°C/min under air flow. The densities (ρ_s) of the HBPIs were measured by a floating method with bromoform and 2-propanol at 25°C. According to the group contribution method, the FFV of HBPIs can be estimated by the following equation [28]:

$$FFV = \frac{V_{sp} - 1.3V_w}{V_{sp}} \quad (1)$$

where V_{sp} (cm³/mol) is the specific molar volume and V_w (cm³/mol) is the van der Waals volume of the repeating unit. CO₂, O₂, N₂, and CH₄ permeation measurements were taken with a constant volume/variable pressure apparatus under 76 cmHg at 25°C. The permeability coefficient, P [cm³(STP)cm/cm² s cmHg], was determined by the equation [29]:

$$P = \frac{22414 L}{A} \frac{V}{p} \frac{dp}{RT dt} \quad (2)$$

where A is the membrane area (cm²), L is the membrane thickness (cm), p is the upstream pressure (cmHg), V is the downstream volume (cm³), R is the universal gas constant (6236.56 cm³ cmHg/mol K), T is the absolute temperature (K), and dp/dt is the permeation rate (cmHg/s). The gas permeability coefficient can be explained on the basis of the solution-diffusion mechanism, which is represented by the equation [30,31]:

$$P = D \times S \quad (3)$$

where D (cm²/s) is the diffusion coefficient and S [cm³(STP)/cm³_{polym} cmHg] is the solubility coefficient. The diffusion coefficient was calculated by the time-lag method represented by the equation [32]:

$$D = \frac{L^2}{6\theta} \quad (4)$$

where θ (s) is the time-lag.

3. RESULTS AND DISCUSSION

3.1. Polymer Synthesis

TADE has asymmetric structure in which two amino groups bind to one of the phenyl group of the diphenyl ether. The reactivity of the amino group in 2-position is lower than other two amino groups. Thus, it is considered that the degree of branching (DB) of the asymmetric HBPI is relatively low and the linearity is

Table 1: Physical Properties of the Asymmetric and Symmetric HBPI-Silica Hybrid Membranes

	η_{inh}^a [dL/g]	Transmittance at 600nm [%]	TMA	DMA	TG-DTA	
			CTE [ppm/°C]	Tg [°C]	T _d ⁵ [°C]	Residue [%]
Asymmetric DA-HBPI	0.27	69.4	47	350	471	0
10wt%SiO ₂	-	88.0	41	390	486	10
20wt%SiO ₂	-	89.3	33	394	492	20
30wt%SiO ₂	-	92.9	28	N.D.	503	30
Asymmetric AM-HBPI	0.56	20.1	45	384	455	0
10wt%SiO ₂	-	24.5	37	385	470	9
20wt%SiO ₂	-	34.7	31	386	478	21
30wt%SiO ₂	-	51.9	25	N.D.	495	30
Symmetric DA-HBPI	0.34	88.9	54	304	457	0
10wt%SiO ₂	-	89.9	47	320	490	10
20wt%SiO ₂	-	90.2	38	338	496	20
30wt%SiO ₂	-	90.3	31	351	509	30
Symmetric AM-HBPI	0.60	50.8	53	366	466	0
10wt%SiO ₂	-	54.4	47	379	477	7
20wt%SiO ₂	-	66.8	41	378	481	20
30wt%SiO ₂	-	76.3	31	N.D.	495	33

^a η_{inh} value on corresponding HBPA.

high. Chen *et al.* reported that the DB of symmetric AM-6FDA-TAPOB HBPI was 0.65 [33]. In our study, the DBs of asymmetric AM-6FDA-TAPB HBPI and symmetric AM-6FDA-TAPOB HBPI measured by a same manner as Chen were 0.25 and 0.65, respectively. This result confirmed that the asymmetric HBPI is more linear than symmetric HBPI.

The η_{inh} values of HBPA are shown in Table 1. In Table 1, it was recognized that the η_{inh} values of TADE system HBPA were lower than those of corresponding TAPOB system HBPA. Generally, it is said that the η_{inh} value of linear-type polymer is higher than that of hyperbranched polymer. Thus, it was expected that the η_{inh} value of TADE system HBPA with lower degree of branching was higher than those of TAPOB system HBPA. However the opposite result was obtained. This might result from the fact that it is difficult to synthesize high molecular weight asymmetric HBPA molecule because of low reactivity of the amino group in 2-position in TADE.

3.2. Polymer Characterization

ATR FT-IR spectra of the asymmetric and symmetric pristine HBPIs, and the asymmetric AM-HBPI-silica hybrid films are shown in Figure 2. The

bands observed around 1784 cm⁻¹ (C=O asymmetrical stretching), 1721 cm⁻¹ (C=O symmetrical stretching), 1360-1374 cm⁻¹ (C-N stretching), and 718-721 cm⁻¹ (C=O bending) are characteristic absorption bands of polyimides [13, 33]. These results indicate that the asymmetric HBPIs are well imidized by thermal imidization at 300°C as well as symmetric HBPIs. The bands around 1857 cm⁻¹ in Figure 2a is attributed to the stretching of C=O of the terminal anhydride groups in the DA-HBPIs [12, 33]. The characteristic band attributed to the stretching of N-H of the terminal amino groups in the AM-HBPIs around 3392cm⁻¹ overlapped with the peak of the O-H groups, and could not be observed. For the HBPI-silica hybrid membranes (Figure 2b), it can be observed that the broad and strong absorption bands around 1100 cm⁻¹ assigned to Si-O-Si stretching are enhanced with increasing SiO₂ content, indicating sufficient formation of the three-dimensional Si-O-Si network [34]. The broad absorption bands around 3480 cm⁻¹ are likely attributed to silanol groups remaining in the silica domain.

The optical transmittances at 600nm are shown in Table 1 and plotted against silica content in Figure 3. The optical transmittances of the pristine asymmetric HBPI films are lower than that of the corresponding

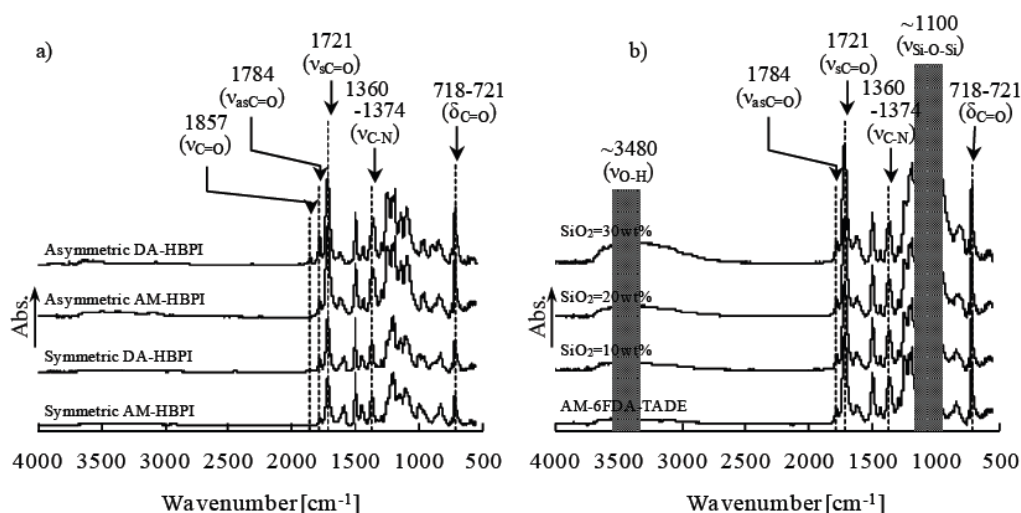


Figure 2: ATR FT-IR spectra of the (a) asymmetric and symmetric HBPIs and (b) asymmetric AM-HBPI-silica hybrids (SiO_2 content: 0-30wt%).

pristine symmetric HBPI films. This is because the molecular size of TADE, a triamine monomer of asymmetric HBPI, is smaller than TAPOB, a triamine monomer of symmetric HBPI, and therefore imide group density in a unit volume of asymmetric HBPI is higher than that of symmetric HBPI. The asymmetric and symmetric AM-HBPI films are colored to dark brown because of the partial thermal denaturation of terminal amino groups of the AM-HBPIs during thermal imidization [26]. However the optical transmittances of asymmetric and symmetric HBPI-silica hybrid films increased with increasing silica content, which might be attributed to decreased imide group density in a unit volume and favorable dispersion of silica. And this

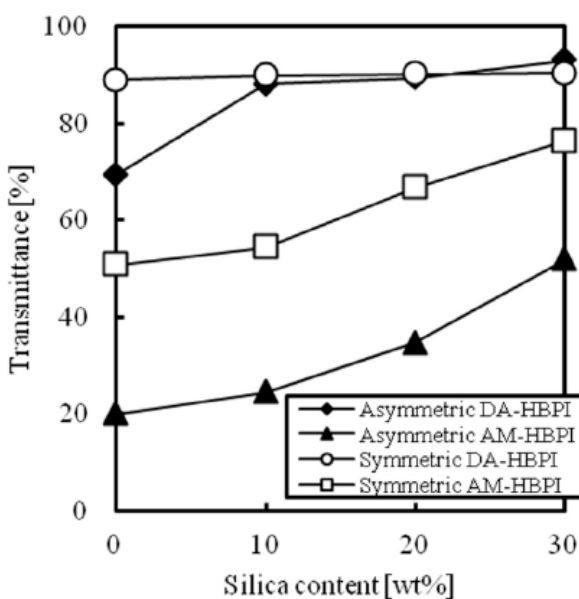


Figure 3: Optical transmittances of asymmetric and symmetric HBPI-silica hybrid films at 600nm.

result indicated the good dispersion of silica component even in the asymmetric HBPI with high linearity. The fine and homogeneous dispersion of silica is brought not only by the characteristic hyperbranched structures of molecular chains but also by silane coupling agent which offer covalent bonds between organic and inorganic components [35].

The thermal properties of the asymmetric and symmetric HBPI-silica hybrids were investigated by TMA, DMA, and TG-DTA measurements. Coefficients of thermal expansion (CTEs) of the asymmetric and symmetric HBPI-silica hybrid films are listed in Table 1 and plotted against silica content in Figure 4. CTE values of the asymmetric HBPI-silica hybrid films were

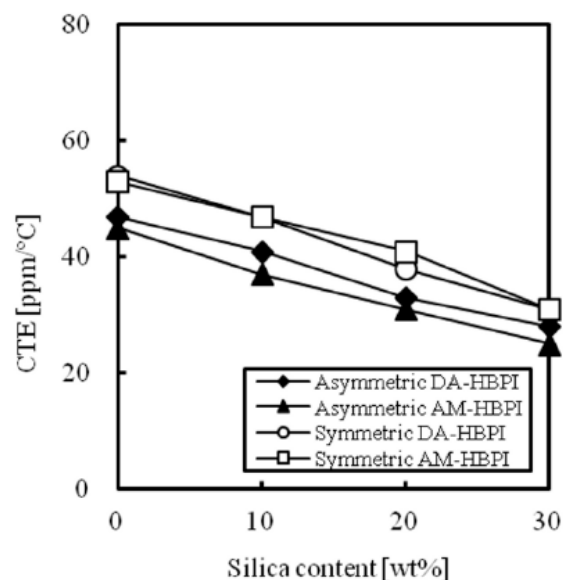


Figure 4: Coefficients of thermal expansion (CTEs) of the asymmetric and symmetric HBPI-silica hybrid films.

lower than those of symmetric HBPI-silica hybrid films. This result is probably caused by the rigidity of the asymmetric HBPI molecular chains. Although only one ether unit is contained in TADE monomer, three ether units are contained in TAPOB monomer. Additionally, the steric hindrance is arisen by the asymmetric structure of TADE. Thus, the asymmetric HBPI molecules are more rigid than the symmetric HBPI molecules. With increasing silica content, CTEs of the asymmetric and symmetric HBPI-silica hybrid films decreased. This is caused by the enhancement of the thermal mechanical stability of the HBPI matrix by the formation of a robust three-dimensional Si-O-Si network and the decreased mobility of the HBPI molecular chains by hybridization with silica.

The Storage moduli (E' s) and $\tan \delta$ of the asymmetric and symmetric HBPI-silica hybrid films are shown in Figure 5a-d. Unfortunately, DMA measurement for the asymmetric DA-HBPI-silica hybrid film containing 30 wt% of SiO_2 could not be carried out because of its mechanical brittleness. In the glassy region, no remarkable difference between the

asymmetric HBPI and the symmetric HBPI was observed. In contrast, in rubbery region, we can see that the E' values of the asymmetric HBPI-silica hybrid films were higher than those of corresponding symmetric HBPI-silica hybrid films. As in the case of CTE, this is attributed to the rigidity of asymmetric (TADE system) HBPI molecules. E' s of the asymmetric and symmetric HBPI-silica hybrid films increased with increasing the silica content in both regions. This increase is caused by the increasing of inorganic behavior and the decreasing of mobility of HBPI molecular chains by hybridization with silica. Glass transition temperatures (T_g s) of the asymmetric and symmetric HBPI-silica hybrid films determined from the peak top of $\tan \delta$ are summarized in Table 1 and plotted against the silica content in Figure 6. The T_g value of asymmetric pristine HBPI is higher than that of corresponding symmetric pristine HBPI. With increasing the silica content, T_g s shifted to a higher temperature along with a decrease of peak intensity and a broadening of the half-width of $\tan \delta$. This result indicates that T_g s increased with the increase of inorganic behavior and the decrease of mobility of the

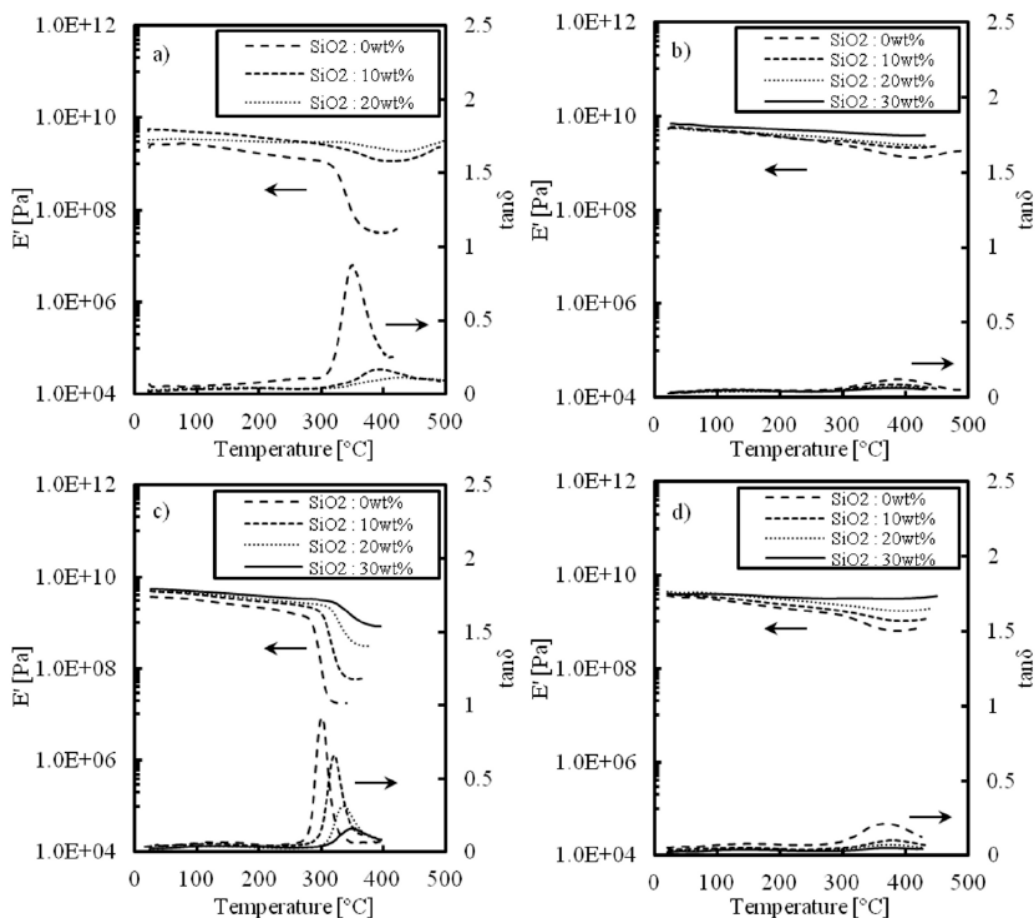


Figure 5: E' and $\tan \delta$ of a) asymmetric DA-HBPI-silica hybrid films, b) asymmetric AM-HBPI-silica hybrid films, c) symmetric DA-HBPI-silica hybrid films and d) symmetric AM-HBPI-silica hybrid films.

HBPI molecular chains caused by crosslinking through silica domains. Particularly, the T_g values of asymmetric and symmetric DA-HBPI-silica hybrids increased with increasing silica content conspicuously. This is probably because that robust three-dimensional Si-O-Si network is easily formed *via* sol-gel reaction in the DA-HBPI-silica hybrids [26].

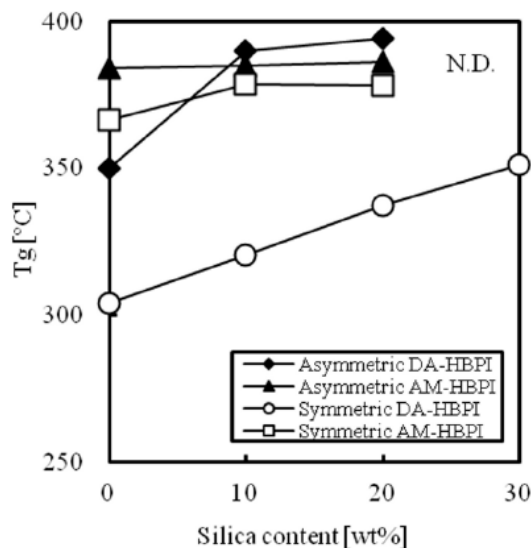


Figure 6: Glass transition temperatures (T_g s) of asymmetric and symmetric HBPI-silica hybrid films derived from the peak tan δ .

5% weight-loss temperatures (T_d^5 s) were investigated by TG-DTA and summarized in Table 1 along with the silica content determined from the residues at 800°C. The residues showed that all hybrid membranes contained an appropriate amount of silica, as expected. In Figure 7, T_d^5 values of the asymmetric and symmetric HBPI-silica hybrids are plotted against silica content. For the symmetric pristine HBPI, the T_d^5 value of the AM-HBPI was higher than that of corresponding DA-HBPI. On the other hand, in the case of asymmetric pristine HBPI, the T_d^5 value of the DA-HBPI was higher than that of corresponding AM-HBPI. T_d^5 values are affected by the amount of thermally unstable units in the molecule. For the symmetric HBPI, the T_d^5 value was probably controlled largely by the degradation of C-F bond in 6FDA component [26]. Thus, the T_d^5 value of the DA-HBPI with higher content of 6FDA was lower than that of AM-HBPI. On the other hand, in the asymmetric HBPI, the rigidity of AM-HBPI molecule may have a major effect on the T_d^5 value. The AM-HBPI is more rigid than DA-HBPI because there are many branching units in the AM-HBPI molecular chains, and so the crosslinking reaction between silane coupling agents is hard to progress and many thermally unstable silanol groups

remain in asymmetric AM-HBPI molecular terminals. The T_d^5 values of the asymmetric and symmetric HBPI-silica hybrid membranes increased with increasing silica content. This increased thermal stability of the HBPI-silica hybrid membranes resulted from the formation of crosslinking between the HBPI and the silica domain, the introduction of inorganic characteristics, and the radical trapping effect of silica. Even though the silica content increased, the T_d^5 of the asymmetric HBPI-silica hybrids did not increase so conspicuously as corresponding symmetric HBPI-silica hybrids. This was probably because there were more silanol groups left in the asymmetric HBPI-silica hybrids than the symmetric HBPI-silica hybrids due to the rigidity of the asymmetric HBPI molecular chains as the above mentioned discussion about the TMA and DMA behaviour.

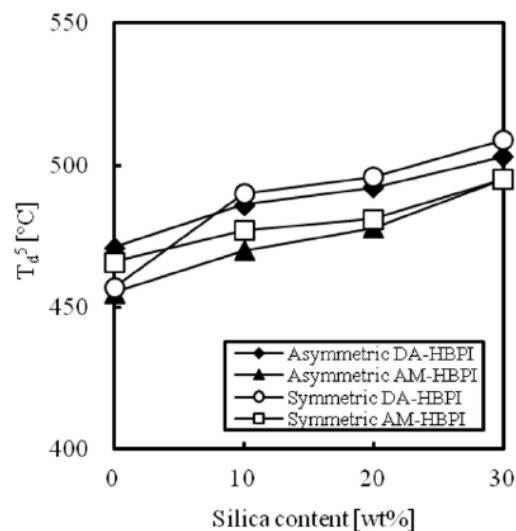


Figure 7: 5% weight loss temperatures (T_d^5 s) of asymmetric and symmetric HBPI-silica hybrids.

3.3. Gas Transport Properties

The gas permeability, diffusion, and solubility coefficients of the asymmetric and symmetric HBPI-silica hybrid membranes are summarized in Table 2 along with the FFVs calculated from the group contribution method. And the CO_2 and CH_4 permeability, diffusion, and solubility coefficients are plotted against silica content in Figures 8a-c and 9a-c, respectively. In general, it is well known that gas diffusivities of polymers strongly depend on the FFVs [36, 37]. In this work, the gas permeabilities and FFVs of asymmetric HBPIs also tended to be higher than those of corresponding symmetric HBPIs. This was due to the higher rigidity of the asymmetric HBPI molecules. As shown in Table 2 and Figure 8, the CO_2 gas

Table 2: Gas Transport Properties of Asymmetric and Symmetric HBPI-Silica Hybrid Membranes at 76cmHg and 25°C

	FFV	$P \times 10^{10}$ [cm ³ (STP)cm/cm ² s cmHg]				$D \times 10^8$ [cm ² /s]				$S \times 10^2$ [cm ³ (STP)/cm ³ polym cmHg]			
		CO ₂	O ₂	N ₂	CH ₄	CO ₂	O ₂	N ₂	CH ₄	CO ₂	O ₂	N ₂	CH ₄
Asymmetric DA-HBPI	0.168	14	2.9	0.43	0.20	0.44	1.9	0.38	0.049	32	1.5	1.1	4.0
10wt%SiO ₂		16	3.1	0.47	0.19	0.45	1.8	0.37	0.045	35	1.7	1.3	4.3
20wt%SiO ₂		18	3.2	0.49	0.18	0.46	1.6	0.31	0.038	39	2.2	1.6	4.6
30wt%SiO ₂		19	3.5	0.46	0.17	0.47	1.6	0.28	0.039	40	2.0	1.7	4.4
Asymmetric AM-HBPI	0.166	18	3.6	0.68	0.22	0.48	1.8	0.57	0.042	38	2.0	1.2	5.3
10wt%SiO ₂		16	3.0	0.56	0.18	0.40	1.6	0.37	0.035	40	1.9	1.5	5.2
20wt%SiO ₂		14	2.4	0.34	0.14	0.34	1.4	0.22	0.021	41	1.8	1.6	6.7
30wt%SiO ₂		13	2.2	0.31	0.10	0.32	0.93	0.20	0.019	42	2.3	1.6	5.3
Symmetric DA-HBPI	0.161	7.4	1.5	0.23	0.098	0.30	1.4	0.25	0.028	25	1.1	0.92	3.5
10wt%SiO ₂		10	2.0	0.31	0.13	0.35	1.5	0.29	0.026	30	1.4	1.1	5.0
20wt%SiO ₂		13	2.1	0.32	0.16	0.37	1.3	0.25	0.030	35	1.7	1.3	5.2
30wt%SiO ₂		23	3.0	0.46	0.24	0.57	1.7	0.29	0.040	41	1.8	1.6	6.0
Symmetric AM-HBPI	0.161	13	2.3	0.35	0.22	0.41	1.5	0.26	0.048	30	1.5	1.3	4.5
10wt%SiO ₂		15	2.4	0.37	0.23	0.47	1.7	0.32	0.055	31	1.4	1.2	4.1
20wt%SiO ₂		16	2.5	0.38	0.22	0.41	1.4	0.27	0.048	38	1.8	1.4	4.6
30wt%SiO ₂		19	2.9	0.43	0.21	0.46	1.5	0.24	0.054	42	1.9	1.8	3.9

permeability coefficient of the asymmetric AM-HBPI-silica hybrid membranes decreased with increasing silica content. In addition, the increasing of the CO₂ gas permeability coefficient of the asymmetric DA-HBPI-silica hybrid membranes with increasing silica content was smaller than those of corresponding symmetric DA-HBPI-silica hybrid membranes. For the CH₄ gas transport property, from Table 2 and Figure 9, it was recognized that the CH₄ gas permeability of the asymmetric HBPI-silica hybrid membranes decreased with increasing silica content conspicuously. And these results on permeability greatly reflect the change in the diffusivity coefficient. In our previous research, we found that the gas permeability coefficient and the CO₂/CH₄ selectivity of the symmetric DA-HBPI-silica hybrid membranes prepared *via* sol-gel reaction using TMOS increased with increasing silica content, suggesting the additional formation of free volume holes and a Langmuir sorption site effective for gas transport and separation properties through hybridization with silica [23,24,38]. However, in the asymmetric HBPI-silica hybrids with the high linearity of polymer chains, the dispersibility of a silica component is not as good as in the symmetric HBPI-silica hybrids. Therefore, silica component is aggregated to the size that affects the gas permeation but doesn't affect the optical transmittance. The more the size of a silica

component is large, the more the diffusion path formed in the PI-silica interfacial region becomes long and tortuous. The effect of newly formed diffusion path was countered by the increase of total path of the gas. Similar gas transport properties have been reported in several other studies. Merkel *et al.* studied the effect of particle size on gas permeability of superglassy polymer-silica nanocomposites. They reported the importance of using small particles to achieve the desired effect on gas transport in the polymer; the gas permeability increases linearly with decreasing silica particle size [39-41]. Dougnac *et al.* also reported similar results about the transport properties of the PA6-silica nanosphere composites [42]. In addition, we have reported that in the AM-HBPI-silica hybrid membranes, it was thought that an effect of hybridization on gas permeability was hard to be taken because of the rigidity of the AM-HBPI polymer chains which inhibit the progress of the sol-gel reaction [26]. It was considered that the rigidity of asymmetric AM-HBPI was the highest of all examined HBPIs, and that the gas permeability decreased with increasing the silica content.

3.4. O₂/N₂ and CO₂/CH₄ Selectivities

The ideal selectivity for the combination of gases A and B [$\alpha(A/B)$] is defined by the equation [43]:

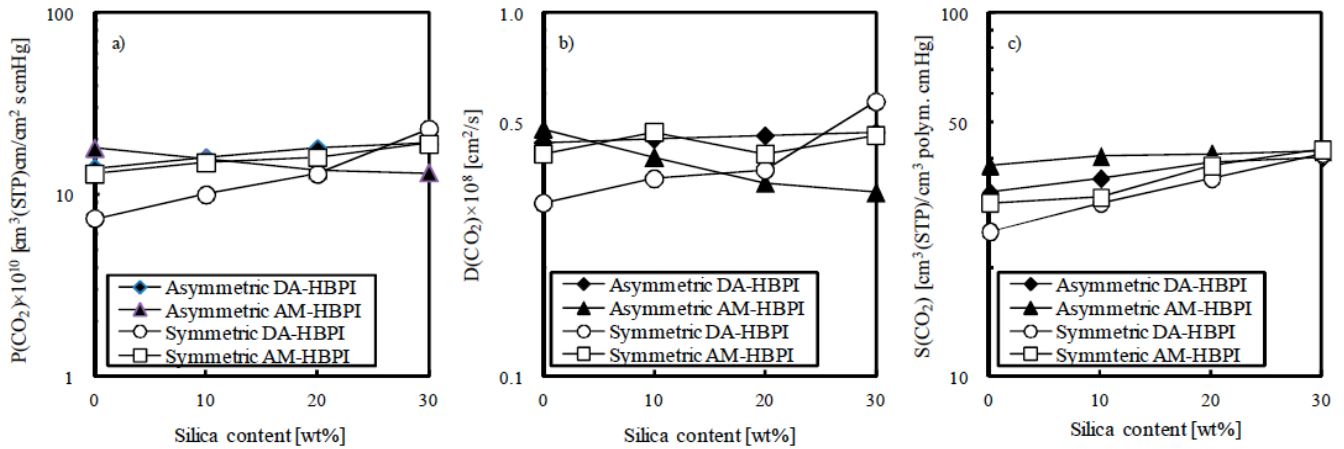


Figure 8: CO₂ a) permeability, b) diffusion and c) solubility coefficients of asymmetric and symmetric HBPI-silica hybrid membranes.

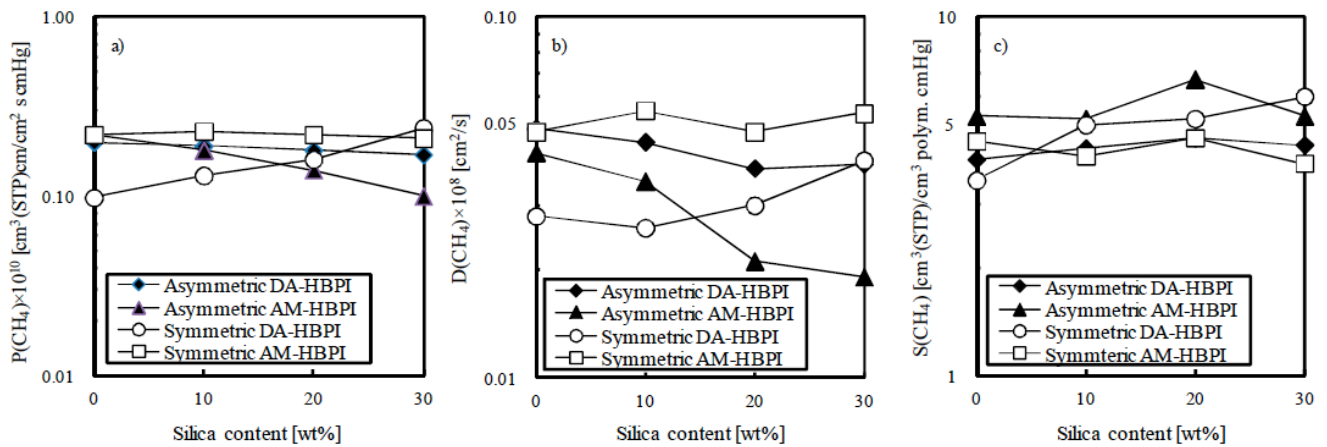


Figure 9: CH₄ a) permeability, b) diffusion and c) solubility coefficients of asymmetric and symmetric HBPI-silica hybrid membranes.

$$\alpha(A/B) = \frac{P(A)}{P(B)} = \frac{D(A)}{D(B)} \times \frac{S(A)}{S(B)} \quad (4)$$

$$= \alpha^D(A/B) \times \alpha^S(A/B)$$

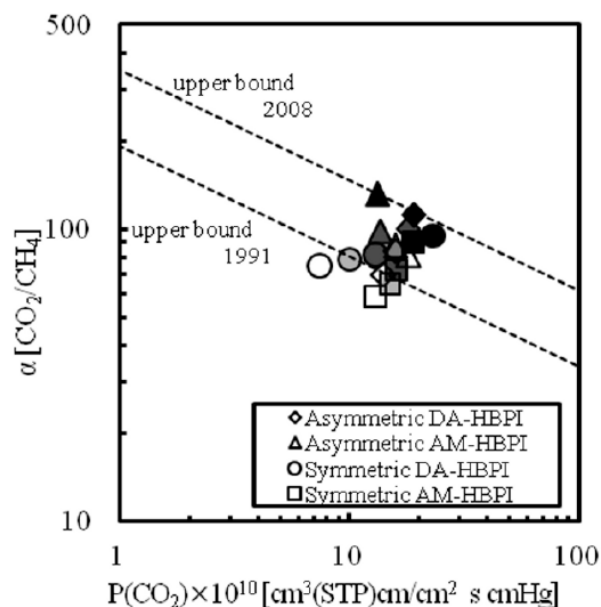
where $\alpha^D(A/B)$ is the diffusivity selectivity and $\alpha^S(A/B)$ is the solubility selectivity. The O₂/N₂ and CO₂/CH₄ selectivities of the HBPI-silica hybrid membranes are listed in Table 3, and $\alpha(\text{CO}_2/\text{CH}_4)$ is plotted against the CO₂ permeability coefficients in Figure 10. In Figure 10, the open symbols represent the data of the pristine HBPI, and the darkness of filled symbols increased with increasing silica content.

In general, there is a trade-off relationship between permeability and permselectivity; the gas selectivity decreases with increasing the permeability, or *vice versa* [43]. In our previous study, we reported that 1) the $\alpha(\text{O}_2/\text{N}_2)$ values of the symmetric DA-HBPI-silica hybrid membranes slightly decreased and the O₂ permeability increased with increasing silica content

along with the upper bound trade-off line for O₂/N₂ separation demonstrated by Robeson [44, 45], and 2) the both $\alpha(\text{CO}_2/\text{CH}_4)$ values and the CO₂ permeability of the symmetric DA-HBPI-silica hybrid membranes increased with increasing silica content. In this study, for the asymmetric AM-HBPI silica hybrid membranes, the plots of the O₂ permeability and O₂/N₂ permselectivity relationship shifted to the low permeability region with increasing silica content along with the upper bound trade-off line. On the other hand, the plots of the CO₂ permeability and CO₂/CH₄ permselectivity relationship shifted to the low permeability region with significant increase of selectivity with the increase of silica content (Figure 10). For this reason, it is considered that the free volume holes formed by hybridization with silica in the asymmetric AM-HBPI silica hybrid membranes have an excellent molecular sieving effect on CO₂/CH₄ selectivity because the CH₄ gas diffusivity coefficient decreased with increasing silica content conspicuously.

Table 3: O₂/N₂ and CO₂/CH₄ Selectivities of Asymmetric and Symmetric HBPI-Silica Hybrid Membranes at 76 cmHg and 25°C

	O ₂ /N ₂ selectivity			CO ₂ /CH ₄ selectivity		
	$\alpha(\text{O}_2/\text{N}_2)$	$\alpha^D(\text{O}_2/\text{N}_2)$	$\alpha^S(\text{O}_2/\text{N}_2)$	$\alpha(\text{CO}_2/\text{CH}_4)$	$\alpha^D(\text{CO}_2/\text{CH}_4)$	$\alpha^S(\text{CO}_2/\text{CH}_4)$
Asymmetric DA-HBPI	6.7	5.0	1.4	70	9.0	8.0
10wt%SiO ₂	6.6	4.9	1.3	84	10.0	8.1
20wt%SiO ₂	6.5	5.2	1.4	100	12	8.5
30wt%SiO ₂	7.6	5.7	1.2	112	12	9.1
Asymmetric AM-HBPI	5.3	3.3	1.7	82	11	7.2
10wt%SiO ₂	5.4	4.3	1.3	88	11	7.8
20wt%SiO ₂	6.0	6.2	1.1	100	16	6.1
30wt%SiO ₂	7.0	4.7	1.5	132	17	7.8
Symmetric DA-HBPI	6.8	5.8	1.2	75	11	7.0
10wt%SiO ₂	6.6	5.2	1.3	79	13	5.9
20wt%SiO ₂	6.7	5.3	1.3	82	12	6.8
30wt%SiO ₂	6.6	5.8	1.1	95	14	6.7
Symmetric AM-HBPI	6.6	5.8	1.2	59	8.5	6.7
10wt%SiO ₂	6.5	5.3	1.2	65	8.6	7.6
20wt%SiO ₂	6.6	5.2	1.3	73	9.5	8.3
30wt%SiO ₂	6.7	6.3	1.1	90	8.5	11

**Figure 10:** Ideal CO₂/CH₄ permselectivity [$\alpha(\text{CO}_2/\text{CH}_4)$] of asymmetric and symmetric HBPI-silica hybrid membranes plotted against CO₂ permeability coefficient.

4. CONCLUSIONS

The asymmetric and symmetric HBPI-silica hybrid membranes were prepared *via* sol-gel reaction and their physical and gas transport properties were

investigated. It is considered that the asymmetric HBPI molecular chain is more linear than symmetric HBPI. ATR FT-IR spectra revealed satisfactory imidization and sufficient formation of a three-dimensional Si-O-Si network in all prepared membranes. The result of optical transmittances indicated the fine and homogeneous dispersion of silica component even in the asymmetric HBPI with high linearity. From the DMA and TMA measurements, it was suggested that thermal and dimensional stability of the asymmetric HBPI-silica hybrids were higher than those of symmetric HBPI-silica hybrids because the rigidity of the asymmetric HBPI molecular chains. Besides, there were more silanol groups left in the asymmetric HBPI-silica hybrids due to the rigidity of the asymmetric HBPI molecular chains. Thus, the T_d^5 values of the asymmetric HBPI-silica hybrids did not increase so conspicuously as corresponding symmetric HBPI-silica hybrids with increasing silica content. The CO₂, O₂, N₂, and CH₄ gas permeability coefficient of asymmetric AM-HBPI-silica hybrid membranes decreased with increasing silica content. This was because the dispersibility of a silica component in the asymmetric HBPI-silica hybrids with the high linearity of polymer chain is not as fine as in symmetric HBPI-silica hybrids, and therefore the long

and tortuous diffusion path was newly formed by hybridization with silica. Nevertheless, the asymmetric HBPI-silica hybrids demonstrate superior CO₂/CH₄ selectivity due to the excellent molecular sieving effect of the newly formed free volume holes by incorporation with silica.

ACKNOWLEDGEMENTS

The authors would like to thank Ministry of Education, Science and Culture for support of the project, Regional Innovation Strategy Support Program, "Kyoto Environmental Nanotechnology Cluster".

REFERENCES

- [1] Kim TH, Koros WJ, Husk GR, O'Brien KC. Relationship between Gas Separation Properties and Chemical Structure in a Series of Aromatic Polyimides. *J Membr Sci* 1988; 37: 45-62. [http://dx.doi.org/10.1016/S0376-7388\(00\)85068-1](http://dx.doi.org/10.1016/S0376-7388(00)85068-1)
- [2] Stern SA, Mi Y, Yamamoto H. Structure/Permeability Relationships of Polyimide Membranes. Applications to the Separation of Gas Mixtures. *J Polym Sci Part B: Polym Phys* 1989; 27: 1887-909. <http://dx.doi.org/10.1002/polb.1989.090270908>
- [3] Okamoto K, Tanaka K, Kita H, Ishida M, Kakimoto M, Imai Y. Gas Permeability and Permselectivity of Polyimides Prepared from 4,4'-Diaminotriphenylamine. *Polym J* 1992; 24: 451-7. <http://dx.doi.org/10.1295/polymj.24.451>
- [4] Li Y, Wang X, Ding M, Xu J. Effects of Molecular Structure on the Permeability and Permselectivity of Aromatic Polyimides. *J Appl Polym Sci* 1996; 61: 741-8. [http://dx.doi.org/10.1002/\(SICI\)1097-4628\(19960801\)61:5<741::AID-APP4>3.0.CO;2-O](http://dx.doi.org/10.1002/(SICI)1097-4628(19960801)61:5<741::AID-APP4>3.0.CO;2-O)
- [5] Hasegawa M, Sensui N, Shindo Y, Yokota R. Structure and Properties of Novel Asymmetric Biphenyl Type Polyimides. Homo- and Copolymers and Blends. *Macromolecules* 1999; 32: 387-96. <http://dx.doi.org/10.1021/ma9808629>
- [6] Hergenrother PM, Watson KA, Smith JG, Connell JW, Yokota R. Polyimides from 2,3,3',4'-Biphenyltetracarboxylic Dianhydride and Aromatic Diamines. *Polymer* 2002; 43: 5077-93. [http://dx.doi.org/10.1016/S0032-3861\(02\)00362-2](http://dx.doi.org/10.1016/S0032-3861(02)00362-2)
- [7] Li Q, Fang X, Wang Z, Gao L, Ding M. Polyimides from Isomeric Oxydiphthalic Anhydrides. *J Polym Sci Part A: Polym Chem* 2003; 41: 3249-60. <http://dx.doi.org/10.1002/pola.10918>
- [8] Sasaki T, Moriuchi H, Yano S, Yokota R. High Thermal Stable Thermoplastic-Thermosetting Polyimide Film by use of Asymmetric Dianhydride (a-BPDA). *Polymer* 2005; 46: 6968-75. <http://dx.doi.org/10.1016/j.polymer.2005.06.052>
- [9] Kim YH. Hyperbranched Polymers 10 Years After. *J Polym Sci Part A Polym Chem* 1998; 36: 1685-98. [http://dx.doi.org/10.1002/\(SICI\)1099-0518\(199808\)36:11<1685::AID-POLA1>3.0.CO;2-R](http://dx.doi.org/10.1002/(SICI)1099-0518(199808)36:11<1685::AID-POLA1>3.0.CO;2-R)
- [10] Gao C, Yan D. Hyperbranched Polymers: from Synthesis to Applications. *Prog Polym Sci* 2004; 29: 183-275. <http://dx.doi.org/10.1016/j.progpolymsci.2003.12.002>
- [11] Jikei M, Kakimoto M. Dendritic Aromatic Polyamides and Polyimides. *J Polym Sci Part A Polym Chem* 2004; 42: 1293-309. <http://dx.doi.org/10.1002/pola.20018>
- [12] Fang J, Kita H, Okamoto K. Hyperbranched Polyimides for Gas Separation Applications. 1. Synthesis and Characterization. *Macromolecules* 2000; 33: 4639-46. <http://dx.doi.org/10.1021/ma9921293>
- [13] Fang J, Kita H, Okamoto K. Gas Permeation Properties of Hyperbranched Polyimide Membranes. *J Membr Sci* 2001; 182: 245-56. [http://dx.doi.org/10.1016/S0376-7388\(00\)00571-8](http://dx.doi.org/10.1016/S0376-7388(00)00571-8)
- [14] Suzuki T, Yamada Y. Synthesis and Gas Transport Properties of Novel Hyperbranched Polyimide-Silica Hybrid Membranes. *J Appl Polym Sci* 2013; 127: 316-22. <http://dx.doi.org/10.1002/app.37893>
- [15] Kicelbick G, Eds. *Hybrid Materials*. Weinheim: Wiley-VCH Verlag GmbH & Co. KgaA 2007.
- [16] Zou H, Wu S, Shen J. Polymer/Silica Nanocomposites: Preparation, Characterization, Properties, and Applications. *Chem Rev* 2008; 108: 3893-957. <http://dx.doi.org/10.1021/cr068035g>
- [17] Cornelius CJ, Marand E. Hybrid Silica-Polyimide Composite Membranes: Gas Transport Properties. *J Membr Sci* 2002; 202: 97-118. [http://dx.doi.org/10.1016/S0376-7388\(01\)00734-7](http://dx.doi.org/10.1016/S0376-7388(01)00734-7)
- [18] Ragosta G, Musto P. Polyimide/silica hybrids via the sol-gel route: High performance materials for the new technological challenges. *eXPRESS Polym Lett* 2009; 3(7): 413-28. <http://dx.doi.org/10.3144/expresspolymlett.2009.51>
- [19] Romero AI, Parentis ML, Habert AC, Gonzo EE. Synthesis of Polyetherimide/Silica Hybrid Membranes by the Sol-gel Process: Influence of the Reaction Conditions on the Membrane Properties. *J Mater Sci* 2011; 46: 4701-9. <http://dx.doi.org/10.1007/s10853-011-5380-4>
- [20] Suzuki T, Yamada Y. Characterization of 6FDA-based Hyperbranched and Linear Polyimide-Silica Hybrid Membranes by Gas Permeation and ¹²⁹XeNMR Measurements. *J Polym Sci Part B Polym Phys* 2006; 44: 291-8. <http://dx.doi.org/10.1002/polb.20692>
- [21] Suzuki T, Yamada Y, Sakai J. Gas Transport Properties of OPA-TAPOB Hyperbranched Polyimide-Silica Hybrid Membranes. *High Perform Polym* 2006; 18: 655-64. <http://dx.doi.org/10.1177/0954008306068228>
- [22] Suzuki T, Yamada Y. Effect of End Group Modification on Gas Transport Properties of 6FDA-TAPOB Hyperbranched Polyimide-Silica Hybrid Membranes. *High Perform Polym* 2007; 19: 553-64. <http://dx.doi.org/10.1177/0954008307081197>
- [23] Suzuki T, Yamada Y. Physical and Gas Transport Properties of Novel Hyperbranched Polyimide-Silica Hybrid Membranes. *Polymer Bulletin* 2005; 53: 139-46. <http://dx.doi.org/10.1007/s00289-004-0322-9>
- [24] Suzuki T, Yamada Y, Itahashi K. 6FDA-TAPOB Hyperbranched Polyimide-Silica Hybrids for Gas Separation Membranes. *J Appl Polym Sci* 2008; 109: 813-19. <http://dx.doi.org/10.1002/app.28145>
- [25] Miki M, Suzuki T, Yamada Y. Structure-Property Relationships of Hyperbranched Polyimide-silica Hybrid Membranes with Different Degree of modification. *J Appl Polym Sci* 2013; 130: 54-62. <http://dx.doi.org/10.1002/app.39011>
- [26] Miki M, Yamada Y. Structure-Gas Transport Property Relationships of Hyperbranched Polyimide-silica Hybrid Membranes. *J Photopolym Technol* 2013; 26(3): 319-26. <http://dx.doi.org/10.2494/photopolymer.26.319>
- [27] Takeichi T, Stille JK. Star and Linear Imide Oligomers Containing Reactive End Caps: Preparation and Thermal Properties. *Macromolecules* 1986; 19: 2093-102. <http://dx.doi.org/10.1021/ma00162a001>
- [28] Van Krevelen DW. *Properties of Polymers*. 3rd ed. Amsterdam: Elsevier 1990; p. 71-107.

- [29] Prabhakar RS, Freeman BD, Roman I. Gas and Vapor Sorption and Permeation in Poly(2,2,4-trifluoro-5-trifluoromethoxy-1,3-dioxole-co-tetrafluoroethylene). *Macromolecules* 2004; 37: 7688-97. <http://dx.doi.org/10.1021/ma048909f>
- [30] Muruganandam N, Koros WJ, Paul DR. Gas Sorption and Transport in Substituted Polycarbonates. *J Polym Sci Part B Polym Phys* 1987; 25: 1999-2026. <http://dx.doi.org/10.1002/polb.1987.090250917>
- [31] Morisato A, Shen HC, Sankar SS, Freeman BD, Pinnau I, Casillas CG. Polymer Characterization and Gas Permeability of Poly(1-trimethylsilyl-1-propyne) [PTMSP], Poly(1-phenyl-1-propyne) [PPP], and PTMSP/PPP Blends. *J Polym Sci Part B Polym Phys* 1996; 34: 2209-22. [http://dx.doi.org/10.1002/\(SICI\)1099-0488\(19960930\)34:13<2209::AID-POLB10>3.0.CO;2-9](http://dx.doi.org/10.1002/(SICI)1099-0488(19960930)34:13<2209::AID-POLB10>3.0.CO;2-9)
- [32] Weinkauff DH, Kim HD, Paul DR. Gas Transport Properties of Liquid Crystalline Poly (p-phenyleneterephthalamide). *Macromolecules* 1992; 25: 788-96. <http://dx.doi.org/10.1021/ma00028a044>
- [33] Chen H, Yin J. Synthesis and Characterization of Hyperbranched Polyimides with Good Organosolubility and Thermal Properties Based on a New Triamine and Conventional Dianhydrides. *J Polym Sci Part A Polym Chem* 2002; 40: 3804-14. <http://dx.doi.org/10.1002/pola.10475>
- [34] Hibshman C, Cornelius CJ, Marand E. The Gas Separation Effects of Annealing Polyimide–Organosilicate Hybrid Membranes. *J Membr Sci* 2003; 211: 25-40. [http://dx.doi.org/10.1016/S0376-7388\(02\)00306-X](http://dx.doi.org/10.1016/S0376-7388(02)00306-X)
- [35] Tomokiyo N, Yamada Y, Suzuki T, Oku. Preparation and Characterization of Hyperbranched Polyimide-Colloidal Silica Hybrids. *J Polym Prep Japan* 2006; 55: 5175-76.
- [36] Park JY, Paul DR. Correlation and Prediction of Gas Permeability in Glassy Polymer Membrane Materials *via* a Modified Free Volume Based Group Contribution Method. *J Membr Sci* 1997; 125: 23-39. [http://dx.doi.org/10.1016/S0376-7388\(96\)00061-0](http://dx.doi.org/10.1016/S0376-7388(96)00061-0)
- [37] Thran A, Kroll G, Faupel F. Correlation Between Fractional Free Volume and Diffusivity of Gas Molecules in Glassy Polymers. *J Polym Sci Part B Polym Phys* 1999; 37: 3344-58. [http://dx.doi.org/10.1002/\(SICI\)1099-0488\(19991201\)37:23<3344::AID-POLB10>3.0.CO;2-A](http://dx.doi.org/10.1002/(SICI)1099-0488(19991201)37:23<3344::AID-POLB10>3.0.CO;2-A)
- [38] Suzuki T, Yamada Y, Tsujita Y. Gas Transport Properties of 6FDA-TAPOB Hyperbranched Polyimide Membrane. *Polymer* 2004; 45: 7167-71. <http://dx.doi.org/10.1016/j.polymer.2004.08.025>
- [39] Merkel TC, Freeman BD, Spontak RJ, He Z, Pinnau I, Meakin P, Hill AJ. Ultrapermeable, Reverse-Selective Nanocomposite Membranes. *Science* 2002; 296: 519-22. <http://dx.doi.org/10.1126/science.1069580>
- [40] Merkel TC, Toy LG, Andrady AL, Gracz H, Stejskal EO. Investigation of Enhanced Free Volume in Nanosilica-Filled Poly(1-trimethylsilyl-1-propyne) by ¹²⁹Xe NMR Spectroscopy. *Macromolecules* 2003; 36: 353-8. <http://dx.doi.org/10.1021/ma0256690>
- [41] Andrady AL, Merkel TC, Toy LG. Effect of Particle Size on Gas Permeability of Filled Superglassy Polymers. *Macromolecules* 2004; 37: 4329-31. <http://dx.doi.org/10.1021/ma049510u>
- [42] Dougnac VN, Peoples BC, Quijada R. The Effect of Nanospheres on the Permeability of PA6/SiO₂ Nanocomposites. *Polym Int* 2011; 60: 1600-06. <http://dx.doi.org/10.1002/pi.3125>
- [43] Freeman BD. Basis of Permeability/Selectivity Tradeoff Relations in Polymeric Gas Separation Membranes. *Macromolecules* 1999; 32: 375-80. <http://dx.doi.org/10.1021/ma9814548>
- [44] Robeson LM. Correlation of Separation Factor versus Permeability for Polymeric Membranes. *J. Membr. Sci.* 1991; 62: 165-85. [http://dx.doi.org/10.1016/0376-7388\(91\)80060-J](http://dx.doi.org/10.1016/0376-7388(91)80060-J)
- [45] Robeson LM. The Upper Bound Revisited. *J. Membr. Sci.* 2008; 320: 390-400. <http://dx.doi.org/10.1016/j.memsci.2008.04.030>